ChemPubSoc Europe

DOI: 10.1002/cssc.201402940

CHEMSUSCHEM Full Papers

Guaiacol Hydrodeoxygenation Mechanism on Pt(111): Insights from Density Functional Theory and Linear Free Energy Relations

Kyungtae Lee,[a] Geun Ho Gu,[a] Charles A. Mullen,[b] Akwasi A. Boateng,[b] and Dionisios G. Vlachos*[a]

Density functional theory is used to study the adsorption of guaiacol and its initial hydrodeoxygenation (HDO) reactions on Pt(111). Previous Brønsted–Evans–Polanyi (BEP) correlations for small open-chain molecules are inadequate in estimating the reaction barriers of phenolic compounds except for the side group (methoxy) carbon-dehydrogenation. New BEP relations are established using a select group of phenolic compounds. These relations are applied to construct a potential-energy surface of guaiacol-HDO to catechol. Analysis shows that catechol is mainly produced via dehydrogenation of the methoxy functional group followed by the CH_x ($x<3$) removal of the functional group and hydrogenation of the ring carbon, in contrast to a hypothesis of a direct demethylation path. Dehydroxylation and demethoxylation are slow, implying that phenol is likely produced from catechol but not through its direct dehydroxylation followed by aromatic carbon-ring hydrogenation.

Introduction

Biomass is a promising sustainable energy resource with potential to reduce dependence on fossil fuels and minimize CO_2 emissions.[1] Specifically, lignocellulosic biomass is the most abundant component in various plants, grass, and residues of agricultural crops.[2] One promising biomass conversion technology is pyrolysis,[3] the thermal decomposition in the absence of added oxygen to produce liquid pyrolysate (bio-oil, pyrolysis oil), biochar, and synthesis gas. The resulting bio-oil differs from conventional fossil fuel oil in heating value, energy density, volatility, viscosity, and corrosiveness due to high oxygen content of 20–50 wt%.[4] For this reason, pyrolysis oil requires catalytic upgrading to reduce the oxygen content before use as blendstock in existing refinery infrastructures. Removal of oxygen from bio-oil can be achieved via hydrodeoxygenation (HDO), which typically requires catalysts operating under high pressure of hydrogen.[5]

Lignocellulosic biomass consists of three main components: cellulose, hemicellulose, and lignin.[4] Among them, lignin has fairly high energy density;[6] pyrolysis of lignin yields up to approximately 30 wt% of phenolic compounds, such as phenols, guaiacols, and syringols.[6b] Various catalysts have been examined for the HDO of phenolic compounds, including Mo-based sulfides, noble metals, and base metals. Mo-based sulfides promoted with Co and Ni are well-known hydrotreating catalysts.[7] However, in order to prevent catalyst deactivation, cofeeding a sulfur-containing species is necessary, which leads to increased sulfur content in bio-oil[4] adding another environmental challenge.

Aside from sulfide-based HDO catalysts, noble metals, such as Ru, Pd, Pt, and Rh, have been actively studied on various supports, for example, Al_2O_3, carbon, MgO. These exhibit better deoxygenation performance compared to sulfide-based catalysts.[8] Recently, Wan et al. compared the HDO performance of *p*-cresol over Pt, Pd, and Ru catalysts supported on Al_2O_3 and carbon.[9] Among them, Pt catalysts showed the highest activity and selectivity in hydrocarbon yields, such as toluene and methyl-cyclohexane. Pt catalysts supported on Al_2O_3 have been examined for guaiacol HDO by Gates and coworkers.[10] According to their experimental results, catechol and phenol were dominant products from guaiacol HDO with selectivity of 50% and 30%, respectively, suggesting that phenol and catechol are produced possibly via demethoxylation and demethylation, respectively. Recently, Gao et al. conducted an experimental study of guaiacol HDO on Pt/C, in which phenol was found to be the most abundant product (40% selectivity) with a relatively small fraction of catechol (10% selectivity).[11] They suggested two possible pathways for phenol production including the direct demethoxylation of guaiacol and the dehydration of catechol.

In this study, we perform density functional theory (DFT) calculations for the HDO of guaiacol to catechol because guaiacol is one of the most abundant phenolic compounds produced from lignin pyrolysis and has structural similarity with coniferyl alcohol (a major constituent of lignin).[12] Guaiacol is also an interesting compound for HDO mechanistic studies as the pres-

[a] Dr. K. Lee, G. H. Gu, Prof. D. G. Vlachos
Catalysis Center for Energy Innovation
Department of Chemical and Biomolecular Engineering
University of Delaware, Newark, DE, 19716 (USA)
E-mail: vlachos@udel.edu

[b] Dr. C. A. Mullen, Prof. A. A. Boateng
Sustainable Biofuels and Coproducts
Eastern Regional Research Center, ARS, USDA
Wyndmoor, PA, 19038 (USA)

Supporting Information for this article is available on the WWW under http://dx.doi.org/10.1002/cssc.201402940.

ence of the hydroxyl and methoxy groups is representative of the large number of oxygen functionalities in lignin-derived bio-oils. In comparison to the simpler phenol, where only dehydroxylation may occur, demethylation and demethoxylation reactions can also play an important role in guaiacol HDO. The construction of a comprehensive reaction mechanism requires considerable computational resources due to the numerous reaction paths that need to be examined. To reduce computational cost, previously reported Brønsted–Evans–Polanyi (BEP) relations for C_1 and C_2 open-chain molecules[13] are assessed and in light of their performance, new BEPs are proposed for phenolic compounds. Finally, possible pathways are proposed and results are compared to experimental data.

Results and discussion

Adsorption configurations and initial reactions of guaiacol

Calculations of the adsorption mode of phenol on Ni(111)[14] and oxygenated aromatics on Pt(111) and Pd(111)[15] suggest flat configurations to be the most favorable. In a previous report, 12 flat adsorption configurations for phenol were compared.[14] We also compared adsorption energies of guaiacol based on 12 flat adsorption modes as well as an additional vertical mode, as shown in Figure S1 and Table S1. We found that the most stable adsorption mode is the bridge A3 or the hcp A2 flat configuration. We chose the bridge A3 mode, which is consistent with the previous phenol result referred to as bridge A2 in Ref. [14], for further studies. As depicted in Figure 1, guaiacol prefers adsorbing on the surface via all aromatic carbon atoms bound to atop/off-atop sites of Pt. The vertical adsorption configuration, which is the most stable mode on Mo-based sulfide and silica surfaces,[16] is the least stable on Pt(111).

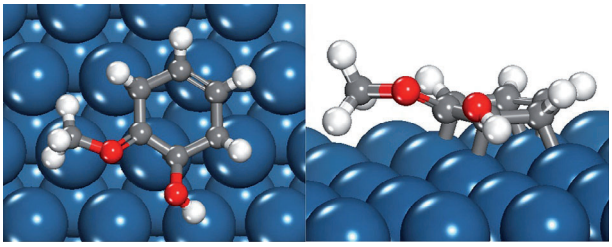

Figure 1. Top and side views of the most preferred adsorption configuration of guaiacol on Pt(111). Large blue spheres, Pt; small gray spheres, C; small red spheres, O; small white spheres, H.

The overall reactions of guaiacol are described in Figure 2 and include dehydrogenation and demethylation of the methoxy group, dehydroxylation, demethoxylation, bond breakage of O–H in the hydroxyl group, and hydrogenation of the aromatic ring. The numbering of the heteroatoms of the ring is also shown.

The energetics of the initial reactions in Figure 3 and Table S2, calculated using DFT, provide insights into the reaction sequence of phenolic compounds. The most favorable reaction path, when activation energy and reaction energy are both considered, is carbon-dehydrogenation of the methoxy side group leading to the R(OH)(OCH_2) intermediate (R stands for the ring). The second favorable path is the dehydrogenation of the OH group leading to the phenoxy radical, but this is expected to be in partial equilibrium due to the considerably low reaction barrier of the reverse reaction. The reaction barriers of ring hydrogenation seem to be quite independent of carbon position and are approximately 1.2 eV. The only exception is the C3 carbon that neighbors the ring carbon bound to the methoxy side group (see numbering in Figure 2), the reaction barrier of which is 0.9 eV. For this reason, in the remainder of this paper we will first consider the ring hydrogenation at the C3 position and compare it to other type of reactions. Another striking point from this energy diagram is that dehydroxylation, demethylation, and demethoxylation, accounting for

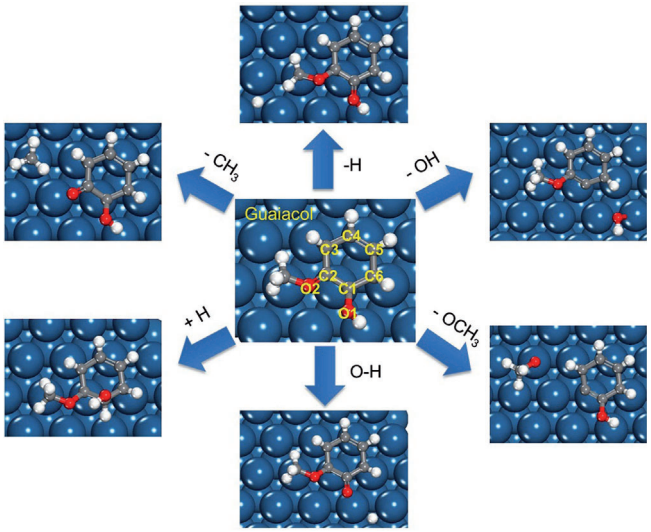

Figure 2. Overall reactions of guaiacol on Pt(111), clockwise from top: dehydrogenation of the methoxy functional group, dehydroxylation, demethoxylation, dehydrogenation of the oxygen (O–H cleavage), ring hydrogenation, and demethylation.

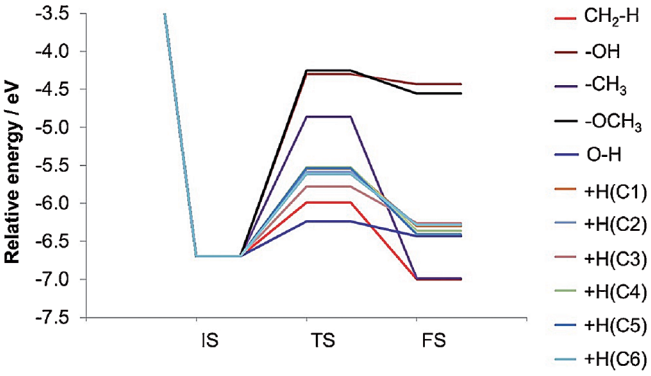

Figure 3. Energy diagram of various reactions of guaiacol on Pt(111) computed using DFT. The relative energy was calculated using Eq. (1). +H(C*x*) represents hydrogenation of the *x*th carbon of the ring; see Figure 2 for numbering of carbons. Dehydrogenation of OH and OCH_3 functional groups is very facile followed by initial ring hydrogenation; dehydroxylation, demethylation, and demethoxylation are very slow.

direct deoxygenation of guaiacol, are energetically much less favorable compared to other reaction paths. This is in line with previous findings[4,17] which suggested that direct deoxygenation is favorable on Mo-based sulfide metals but not on transition metals.

Demethylation and demethoxylation were previously hypothesized to be key reaction paths during guaiacol HDO;[10b] since direct paths are not preferred, according to our energy profile in Figure 3, we considered also the effects of initial state configuration and ring saturation level. Since a weaker chemical bond is implicitly associated with easier bond dissociation, we searched for adsorption configurations containing the longest O–CH_3 (for demethylation) and C_{ring}–OCH_3 (for demethoxylation) bonds of guaiacol, where C_{ring} represents the carbon atom of the phenolic ring. According to Table S3 (listing all bond length data), the longest bond lengths in the O–CH_3 and C_{ring}–OCH_3 bonds of guaiacol are found in fcc A2 and bridge A2 adsorption modes, respectively. Table 1 provides the activation, binding, and reaction energies for demethylation and demethoxylation, comparing the adsorption mode corresponding to the longest bond length with the most stable bridge A3 mode. The values indicate no significant change in energetics with adsorption configuration.

Table 1. Binding energies ΔE_{ads}, activation energies E_a, and reaction energies ΔE_{rxn} of demethylation and demethoxylation of guaiacol at two different adsorption configurations of guaiacol on Pt(111).

	Demethylation				Demethoxylation		
Adsorption mode	ΔE_{ads} [eV]	E_a [eV]	ΔE_{rxn} [eV]	Adsorption mode	ΔE_{ads} [eV]	E_a [eV]	ΔE_{rxn} [eV]
fcc A2	−2.35	1.88	−0.27	bridge A2	−2.31	2.52	1.45
bridge A3	−2.41	1.83	−0.28	bridge A3	−2.41	2.44	2.12

Next, we probed the effect of ring saturation on the demethylation barrier to determine if ring activation is a prerequisite for this reaction to take place. The reaction barriers of four different compounds with varying ring-saturation level were compared. The images of initial, transition, and final states are illustrated in Figure S2. As shown in Table 2, there is almost no difference in activation energies even though the reaction exothermicity increases with increasing ring saturation level. Thus, our results imply direct demethylation and demethoxylation are unlikely to occur during guaiacol HDO. In addition, ring activation does not look relevant to these paths.

Table 2. Effect of ring saturation level on demethylation barriers E_a and reaction energies ΔE_{rxn} on Pt(111). R stands for benzene ring, the numbers in front of hydrogen in parenthesis indicate the hydrogenated ring-carbon position(s), and the subscript indicates the number of added hydrogens to the ring. Breaking the aromaticity has little effect on the demethylation barrier.

Reactant	E_a [eV]	ΔE_{rxn} [eV]
R(OH)(OCH_3)	1.83	−0.28
R(3 H)(OH)(OCH_3)	1.82	−0.27
R(36H_2)(OH)(OCH_3)	1.82	−0.45
R(3456H_4)(OH)(OCH_3)	1.75	−0.54

In order to reconcile the experimental findings, and given that dehydrogenation of the methyl group is facile (Figure 3), we have explored whether side group dehydrogenation could be an effective way leading to removal of the CH_3 and OCH_3 groups. Previous work in open chain molecules, such as ethanol, ethylene glycol, and glycerol, where removal of a few hydrogen atoms facilitates C–C bond scission; yet, no significant C–O bond scission was observed in microkinetic calculations of those molecules.[18] Whether this finding extends to side groups of aromatics and specifically to C–O bond breaking is unknown. For this reason, various dehydrogenation levels of the methoxy functional group were examined to identify the most favorable one in the removal of the CH_x and OCH_x groups, where x ranges from 1 to 3. The surface species considered are depicted in Figure 4 and the energy data for the removal of CH_x and OCH_x groups are compared in Figure 5 with the images of the transition and final states in Figure S3. For OCH_x removal, both reaction energy and reaction barrier are slightly more favorable when x is 1, but the reaction is still highly endothermic with a significant reaction barrier. Consequently, it is unlikely that direct demethoxylation of guaiacol on Pt(111) occurs. We propose a possible indirect path later in the paper. On the other hand, the activation energy of CH_x removal

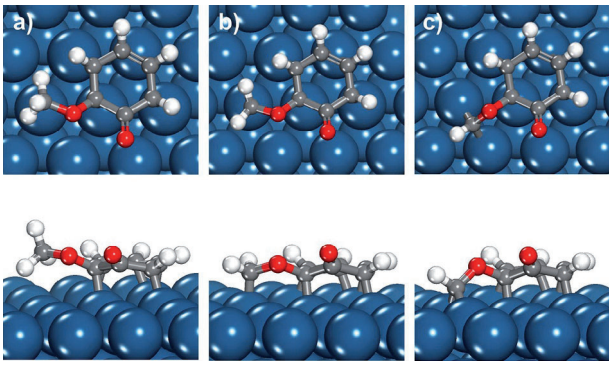

Figure 4. Top and side views of adsorption structures of a) R(O)(OCH_3), b) R(O)(OCH_2), and c) R(O)(OCH). R stands for the ring.

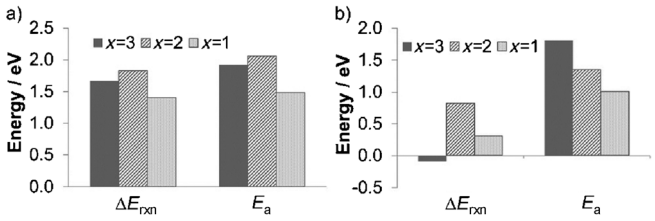

Figure 5. Comparison of reaction energies ΔE_{rxn} and activation energies E_a for the removal reaction of a) the OCH_x and b) CH_x from the OCH_x side group of R(O)(OCH_x). R stands for the ring. The degree of saturation of the side group has a slight effect on demethoxylation whereas the less saturated the carbon of the side group is, the easier the demethylation is.

continuously decreases as x decreases; at $x=1$ the reaction barrier for CH_x removal is 0.5 eV lower than that for OCH_x removal. In addition, the reaction energy at $x=1$ is only slightly endothermic. Thus, CH_x removal is more likely to occur than OCH_x removal and requires dehydrogenation steps before the C–O scission occurs. This indicates that the rate-determining step in demethylation is actually the dehydrogenation of the methyl group.

BEP relations

The mechanistic study of guaiacol HDO, and of other large phenolic molecules, can be facilitated using BEP relations that, once developed, eliminate the computational cost required to locate numerous transition states. BEP relations for linear oxygenated molecules on Pt(111) were previously reported,[13] but their applicability for phenolic ring compounds remains unproven. BEP relations for other classes of biomass molecules have also been proposed.[19] An interesting question is whether BEPs developed for small molecules apply to cyclic biomass compounds. For example, BEP relations developed recently for furanics on Pd(111) showed that errors can be reduced using BEP relations developed specifically for those compounds.[20]

Figure 6 quantifies the errors in applying the existing BEP relations[13] for various reactions that likely occur in guaiacol. The errors for ring hydrogenation and demethylation are less than 0.3 eV compared to the DFT-calculated reaction barriers in Figure 3. However, the accuracy of the BEP relations for dehydroxylation, demethoxylation, and O–H dehydrogenation needs to be improved. To establish BEP relations for phenolic compounds, the barriers of several reactions, listed in Table S4, were computed using DFT. From the regression of reaction energies and activation energies in Figure 7, we found that oxygen breaking from the ring carbon in dehydroxylation and demethoxylation as well as the CH_x removal from the O–CH_x functional group can be lumped together into a single BEP relation denoted as C_{ring}–OA/C_{ring}O–CH_x (A = H or CH_x, x = 1,2). Demethylation reactions denoted as O–CH_3 (i.e., the CH_3 removal from the C_{ring}O–CH_3 functional group), on the other hand, constitute another BEP relation because the methoxy group is only attached to the aromatic ring in contrast to OCH_x (x = 1, 2) functional group that is bound to both the aromatic ring and the metal surface.

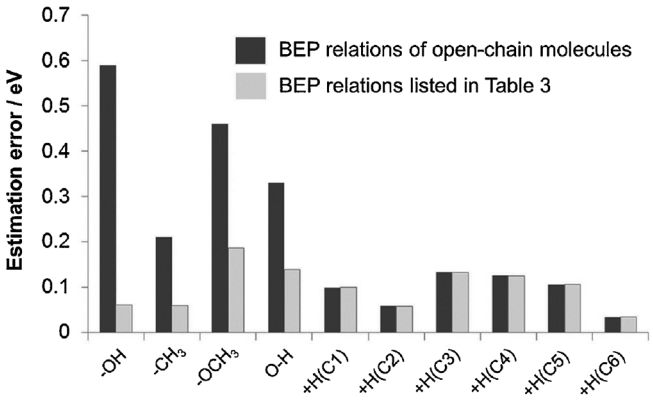

Figure 6. Deviation of activation energies of various reactions of guaiacol estimated using the BEP relations of open-chain molecules (dark gray bars) and the BEP relations listed in Table 3 (light gray bars) on Pt(111) from the actual DFT values. In the BEPs, DFT-calculated heats of reaction were employed. +H(Cx) represents hydrogenation of the xth carbon of the ring; see Figure 2 for numbering of carbons.

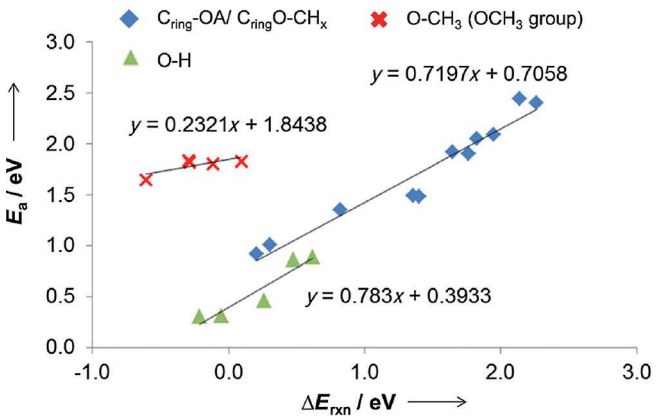

Figure 7. BEP plots relating activation energy to reaction energy for carbon-oxygen bond scission in C_{ring}–OA/C_{ring}O–CH_x (A is H or CH_x, x = 1,2), C–O bond breaking of the O–CH_3 functional group, and O–H bond breaking of the OH functional group on Pt(111). The reactions considered are listed in Table S3.

In summary, the BEP relations for phenolic compounds can be grouped into four families listed in Table 3; among these, the existing BEP relations of open-chain molecules work for C–H dehydrogenation of the aromatic ring carbons and substituent groups.[13] The mean and maximum absolute errors of these newly established BEP relations are low (below 0.1 and 0.3 eV, respectively). These BEP relations can be applied to different facets or stepped surfaces as long as the structures remain the same as studied here. Different surfaces are known to result in data scatter around a BEP line and the extent of scattering depends on the reaction class.[21] It is also quite common to use the same BEPs on different metals (see review[22]). For higher accuracy, a shift in the terrace BEP-intercept may be necessary to apply to stepped-surfaces.

Table 3. BEP correlation parameters for phenolic compounds on Pt(111) along with mean and max absolute errors (AE). Unlike the other reaction families, the O–CH_3 family has an early transition state.

	α	β [eV]	Mean AE [eV]	Max AE [eV]
C–H[a]	1.02	1.06	0.11	0.25
C_{ring}–OA/C_{ring}O–CH_x (A = H, CH, or CH_2)	0.72	0.71	0.09	0.23
O–CH_3 (OCH_3 group)	0.23	1.84	0.04	0.06
O–H	0.78	0.39	0.07	0.14

[a] Taken from Ref. [13].

Extended reaction network

Path searching and mechanism generation of surface kinetics have significantly been advanced in recent years. For the former, we have proposed use of semi-empirical methods to compute thermochemistry via group additivity and reaction barriers using BEPs to eliminate unstable intermediates and very slow parallel reactions and reduce the reaction network a priori, that is, prior to performing microkinetic modeling.[23] For the latter, automatic mechanism generation codes have been developed, for example, rule input network generator (RING),[24] that input families of feasible elementary reactions and create a network with complete enumeration of all paths. Combination of these two approaches can be powerful for constructing and containing the size of reaction mechanisms. A necessary ingredient in using automatic mechanism generation is identification of feasible elementary reactions. For example, inclusion of direct demethylation and demethoxylation, as the only elementary steps of removal of side groups of lignin compounds on metal surfaces, would lead to an incomplete and experimentally irrelevant network, as our work shows. It is our thesis that initial DFT work on pathways and BEPs, as demonstrated here, should precede full path searching and mechanism generation to leverage and enhance their power. Our approach here emphasizes the elementary reactions and paths that one should consider in the aforementioned methods. Another powerful technique for a posteriori identification of key pathways is microkinetic modeling.[22] It requires inclusion of all paths and parameterization of all reaction constants and thermochemistry, a rather daunting task for large mechanisms for which little information is known. As a result, it is often the last method used among path searching methods. We propose that these tools can be used in a symbiotic manner. For example, in this work we performed initial microkinetic modeling (not shown) by considering only the direct demethylation and demethoxylation paths, and the activity was orders of magnitude lower compared to experiments. It was clear that we had missed reaction paths in our network and this motivated our follow-up DFT and BEP works presented herein. This point supports our earlier comment that it is best to perform mechanism generation and microkinetic modeling in concert with DFT and BEP work. With this in mind, herein we made a list of possible reactions based on previous reports regarding HDO of phenolic compounds, as discussed in Figure 2, and considered likely dissociation reactions if a side group is adjacent to the catalyst surface (given that direct demethylation and demethoxylation are unfavorable on Pt). This approach enabled us to include dehydrogenation of the methoxy functional group. The energetics of key reactions from guaiacol were compared to determine the preferred reaction path, as described in Figure 3. Similar reactions were also exploited in other intermediates due to their structural similarity to guaiacol. Path searching methods can build upon the work we present here as part of future work.

As discussed above, guaiacol, R(OH)(OCH_3), undergoes initially methyl dehydrogenation, leading to R(OH)(OCH_2). A number of subsequent steps beyond the initial reactions depicted in Figure 3 were also examined in Figure S4. To reduce computational cost, (1) the BEP relations listed in Table 3 were utilized to find favorable reaction paths using DFT-computed reaction energies and (2) hydrogenation of the ring was examined only at the C3 position as a model reaction since it was found to be the most favorable ring hydrogenation step (Figure 3).

Upon formation of the R(OH)(OCH_2), dehydrogenation of OH has the lowest reaction barrier, leading to R(O)(OCH_2) (Figure S4b). Since this O–H breaking step is thermo-neutral, this reaction is likely to be in partial equilibrium. Other possible paths from R(OH)(OCH_2) were also examined; the most favorable ones include the dehydrogenation of CH_2 and the CH_2 removal both of which are potentially also in partial equilibrium due to being thermo-neutral. According to Figure S4b and c, both reaction paths prefer forming R(OH)(O) and then catechol, R(OH)(OH). Thus, energetics indicate that there is no unique preferred pathway leading to catechol. For this reason, we traced the next reaction paths of R(O)(OCH_2) where the dehydrogenation of the OCH_2 functional group is favored, as shown in Figure S4d. The C–O cleavage of the OCH functional group finally takes place fairly easily, as shown in Figure 5. After R(O)(O) forms, sequential hydrogenations of the ketone groups are preferred because breaking of a ketone group is energetically disfavored, as shown in Figure S4d.

The most energetically favorable reaction path from guaiacol to catechol is summarized in Figure 8 and Table S5. All activation energies are lower than 1 eV and the overall reaction is

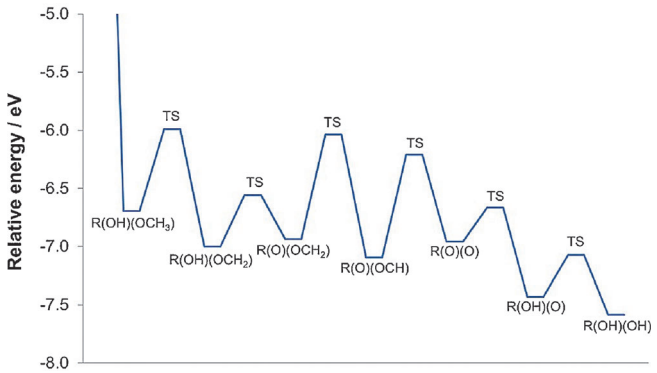

Figure 8. Lowest energy diagram of catechol production from guaiacol on Pt(111). R stands for the ring. Additional possible pathways are shown in Scheme 1. Adsorption energies are DFT values and transition state energies are estimated using BEP relations.

downhill, implying that this reaction path is thermodynamically and kinetically preferred. In addition to this path, other paths discussed above may also be competitive. A simple reaction network for guaiacol HDO on Pt(111), which considers these paths, is illustrated in Scheme 1. As discussed in Figure S4, R(OH)(OCH_2) can lead to the R(O)(OH) intermediate via three reactions. Main differences between paths entail whether CH or CH_2 is being removed from the side group and whether the intermediate, from which the side group departs, consists of an OH or a carbonyl group.

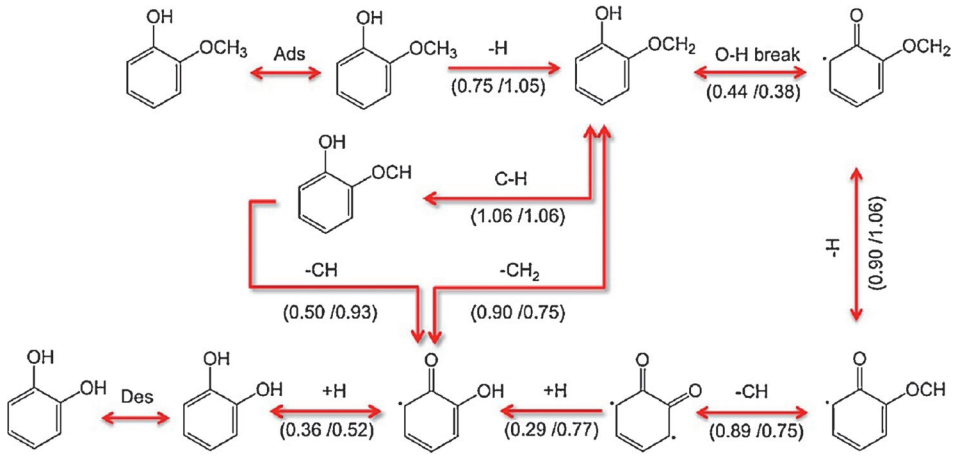

Scheme 1. Proposed reaction network for the conversion of guaiacol to catechol on Pt(111). The values in parenthesis indicate the activation energies (in eV) for forward/reverse reactions estimated using BEP relations. Reversible (irreversible) reactions are indicated by double (single) headed arrows.

The reaction network in Scheme 1 is consistent with the experimental observation where catechol is a major product on Pt/γ-Al_2O_3; however, it cannot explain why phenol is a second major product.[10b] Since the energetics of direct OCH_x (x = 1,2,3) removal is unfavorable (Figure 5a and Figure S4), phenol is probably produced from catechol via dehydration on alumina, which is a well-known catalyst for dehydration reaction of alcohols,[25] along with hydrogenation on the metal. Dehydration of catechol was also experimentally suggested to be a feasible reaction path for phenol production.[11] The mechanistic details of catechol conversion to phenol need to be understood in future work. In our mechanism, catechol formation proceeds from demethylation enabled by sequential dehydrogenation steps of the functional group. Experimentally, the product stream also contains various minor products, formed via transalkylation, such as 3-methyl catechol, 6-methyl guaiacol, 3-methyl guaiacol, and *o*-cresol. Possible mechanisms may be inferred from DFT energetics and a better understanding will require microkinetic modeling. Transalkylation products could be generated from the CH_3 fragment produced by H and CH surface species detached from the methoxy functional group but their production may be limited by a likely high reaction barrier for dehydrogenation of phenolic rings[26] or the availability of CH_x species given their potential consumption to methanol. For example, according to our calculations, ring carbon dehydrogenation of catechol on Pt(111) is an endothermic reaction (reaction energy of 0.9 eV) with a high reaction barrier (BEP-estimated reaction barrier of 1.9 eV). Additional minor products include veratrole and anisole that may be produced from catechol and phenol with an exchange between the H atom of the OH functional group and the CH_3 surface species due to a relatively less endothermic process and low reaction barrier of O–H cleavage as shown in the last step of the energy diagram of Figure 8. For instance, the reaction energy and BEP-estimated reaction barrier for O–H cleavage of phenol on Pt(111) were calculated to be 0.1 and 0.5 eV, respectively, indicating that while dehydrogenation of OH is feasible, the reaction is reversible, and the availability of oxygen for addition of another functional group, for example, CH_3, will be low especially in excess of hydrogen.

The reaction mechanism proposed herein is under gas-phase conditions. An aqueous environment would result in differences in the guaiacol HDO mechanism. As an example, previous studies of phenol HDO in an acidic aqueous medium proposed ring hydrogenation followed by the removal of the hydroxyl group.[27] It is entirely possible that similar paths exist also for guaiacol HDO in an aqueous medium. In addition, there is growing body of work supporting keto/enol tautomerization in aqueous acid medium[27b] with low reaction barriers in contrast to vapor phase kinetics discussed herein. Our work and those in aqueous medium underscore the importance of solvent effects and acidity that need to be better understood for closing the gap between vapor and liquid phase experimental studies.

Conclusions

We have investigated the reaction mechanism of guaiacol hydrodeoxygenation (HDO) to catechol on Pt(111) using DFT calculations in conjunction with linear free energy or Brønsted–Evans–Polanyi (BEP) relations. The previously reported BEP relations for open-chain molecules were generally found to be inadequate for guaiacol HDO. We proposed BEP relations for four reaction families, namely C–H bond scission (this family only follows the open-chain molecules), C–O bond scission in C_{ring}–OA/$C_{ring}O$–CH_x (A = H, CH_x x = 1,2), O–CH_3 bond scission, and O–H bond scission. The maximum absolute error of these BEPs is less than 0.3 eV.

These BEP relations were utilized to construct a potential energy surface of guaiacol HDO on Pt(111), suggesting that guaiacol undergoes dehydrogenation of the methoxy group rather than direct de-oxygenation (i.e., C–O bond breaking) via dehydroxylation, demethylation, and demethoxylation. Upon single or double dehydrogenation of the methyl group, O–CH_x bond scission occurs easily followed by hydrogenation of the oxygen(s) attached to the ring. The resulting catechol desorbs as a major product or undergoes HDO to produce phenol. The last step may happen at the Pt/alumina interface, where alumina removes the OH and Pt carries out the necessary hydrogenation. Our proposed guaiacol reaction mechanism on Pt(111) does not support the hypothesis invoking direct demethylation and demethoxylation in converting guaiacol to catechol and phenol. Future DFT calculations of the HDO chemistry of guaiacol on stepped surfaces will be needed to explore the role of

steps in direct demethylation and demethoxylation of catechol to phenol and the role of enol/keto tautomerization. These additional DFT studies along with microkinetic simulations and suitable experiments will provide further insights into the reaction mechanism of HDO of lignin derivatives.

Experimental Section

Computational Methods

All calculations were carried out using the Vienna ab initio simulation program (VASP, version 5.2.12).[28] The exchange and correlation energies were incorporated using the Perdew–Burke–Ernzerhof functional with the latest dispersion correction, PBE-D3.[29] The projector augmented wave (PAW) method of Blöchl was used for the electron-ion interactions.[30] The cutoff energy of 400 eV was applied for a plane-wave basis set to represent valence electrons. All gas-phase molecules were optimized in a $20\times20\times20$ Å unit cell. Geometry optimizations were considered to be converged when the forces on all atoms were less than 0.05 eV Å^{-1}. The optimized lattice constant for the fcc Pt crystal was 3.92 Å, which is consistent with the experimental value.[31] The Pt surface was terminated by the (111) facet with a 4×4 cell size and a vacuum region of 20 Å normal to the surface. The Pt metal slab was composed of four atomic layers with the top two layers relaxed, and the Brillouin zone was sampled with a $5\times5\times1$ Monkhorst–Pack k-point grid.[32] Transition states were optimized using the climbing image nudged elastic band (CI-NEB) method.[33] The CI-NEB was implemented by interpolating four images between the initial and final states and optimizing the images along the reaction coordinate. Each transition state was confirmed from the presence of an imaginary vibrational frequency at the maximum energy value.

The adsorption energy was calculated as $\Delta E_{ads}=E_{slab+i}-E_{slab}-E_i$, where E_{slab+i} is the energy of the metal slab–adsorbate system, E_{slab} is the energy of a clean slab, and E_i is the gas-phase energy of the adsorbate. Relative molecular binding energies were calculated based on the energy sum of guaiacol gas ($C_7H_8O_2$), hydrogen gas (H_2), and the Pt surface. For example, the binding energy of phenol (C_6H_6O) is expressed as

$$C_7H_8O_2\ (g)+4H_2\ (g)+*\rightarrow C_6H_6O^*+7\,H^*+OCH_3^*$$

$$\begin{aligned}\Delta E(C_6H_6O^*) = {} & E(C_6H_6O^*/\text{Pt Surface})\\ & +7\times[E(H^*/\text{Pt surface})-E(\text{Pt surface})]\\ & +[E(OCH_3^*/\text{Pt surface})-E(\text{Pt surface})]\\ & -E(C_7H_8O_2)-4\times E(H_2)-E(\text{Pt Surface})\end{aligned}\qquad(1)$$

BEP relations developed herein are used to estimate reaction barriers by correlating the activation energy E_a with the reaction energy ΔE_{rxn} as

$$E_a=\alpha\Delta E_{rxn}+\beta\qquad(2)$$

where α and β are the slope and intercept, respectively.

Acknowledgements

K.L. performed most of the DFT calculations and wrote up the paper. G.H.G. assisted with computing some of the transition states and refining some of the calculations. D.G.V. conceptualized this research and advised the research direction and the paper writing. We would like to thank Vassili Vorotnikov for useful discussions. The DFT work of K. L. and G. H. G. was supported by the USDA-NIFA-BRDI grant 2012-10008-20271 and the BEP development of K. L. was supported by the US Department of Energy, Energy Efficiency and Renewable Energy's Bioenergy Technologies Office with Pacific Northwest National Laboratory (PNNL). PPNL is operated by Battelle for the US Department of Energy. DFT calculations were carried out in part using the TeraGrid resources provided by the Texas Advanced Computing Center (TACC) of the University of Texas at Austin and using the resources of the National Energy Research Scientific Computing Center (NERSC).

Keywords: biomass · DFT · guaiacol · hydrodeoxygenation · platinum

[1] J. N. Chheda, G. W. Huber, J. A. Dumesic, *Angew. Chem. Int. Ed.* **2007**, *46*, 7164–7183; *Angew. Chem.* **2007**, *119*, 7298–7318.
[2] C. H. Zhou, X. Xia, C. X. Lin, D. S. Tong, J. Beltramini, *Chem. Soc. Rev.* **2011**, *40*, 5588–5617.
[3] T. Dickerson, J. Soria, *Energies* **2013**, *6*, 514–538.
[4] H. M. Wang, J. Male, Y. Wang, *ACS Catal.* **2013**, *3*, 1047–1070.
[5] P. M. Mortensen, J. D. Grunwaldt, P. A. Jensen, K. G. Knudsen, A. D. Jensen, *Appl. Catal. A* **2011**, *407*, 1–19.
[6] a) S. Czernik, A. V. Bridgwater, *Energy Fuels* **2004**, *18*, 590–598; b) C. Zhao, J. Y. He, A. A. Lemonidou, X. B. Li, J. A. Lercher, *J. Catal.* **2011**, *280*, 8–16; c) D. Mohan, C. U. Pittman, P. H. Steele, *Energy Fuels* **2006**, *20*, 848–889.
[7] a) O. I. Şenol, E. M. Ryymin, T. R. Viljava, A. O. I. Krause, *J. Mol. Catal. A* **2007**, *277*, 107–112; b) O. I. Şenol, T. R. Viljava, A. O. I. Krause, *Catal. Today* **2005**, *100*, 331–335; c) Y. Romero, F. Richard, S. Brunet, *Appl. Catal. B* **2010**, *98*, 213–223.
[8] J. Wildschut, F. H. Mahfud, R. H. Venderbosch, H. J. Heeres, *Ind. Eng. Chem. Res.* **2009**, *48*, 10324–10334.
[9] H. J. Wan, R. V. Chaudhari, B. Subramaniam, *Top. Catal.* **2012**, *55*, 129–139.
[10] a) T. Nimmanwudipong, R. C. Runnebaum, D. E. Block, B. C. Gates, *Catal. Lett.* **2011**, *141*, 779–783; b) T. Nimmanwudipong, R. C. Runnebaum, D. E. Block, B. C. Gates, *Energy Fuels* **2011**, *25*, 3417–3427; c) T. Nimmanwudipong, C. Aydin, J. Lu, R. C. Runnebaum, K. C. Brodwater, N. D. Browning, D. E. Block, B. C. Gates, *Catal. Lett.* **2012**, *142*, 1190–1196; d) R. C. Runnebaum, T. Nimmanwudipong, D. E. Block, B. C. Gates, *Catal. Sci. Technol.* **2012**, *2*, 113–118.
[11] D. Gao, C. Schweitzer, H. T. Hwang, A. Varma, *Ind. Eng. Chem. Res.* **2014**, DOI: 10.1021/ie500495z.
[12] a) J. Zakzeski, P. C. A. Bruijnincx, A. L. Jongerius, B. M. Weckhuysen, *Chem. Rev.* **2010**, *110*, 3552–3599; b) N. Yan, C. Zhao, P. J. Dyson, C. Wang, L. T. Liu, Y. Kou, *ChemSusChem* **2008**, *1*, 626–629; c) T. J. Chen, C. J. Deng, R. H. Liu, *Energy Fuels Energy Fuel* **2010**, *24*, 6616–6623.
[13] J. E. Sutton, D. G. Vlachos, *ACS Catal.* **2012**, *2*, 1624–1634.
[14] L. Delle Site, A. Alavi, C. F. Abrams, *Phys. Rev. B* **2003**, *67*, 193406.
[15] J. Yang, P. J. Dauenhauer, A. Ramasubramaniam, *J. Comput. Chem.* **2013**, *34*, 60–66.
[16] a) M. Badawi, J. F. Paul, S. Cristol, E. Payen, *Catal. Commun.* **2011**, *12*, 901–905; b) K. Johnston, A. Gulans, T. Verho, M. J. Puska, *Phys. Rev. B* **2010**, *81*, 235428.
[17] Y. C. Lin, C. L. Li, H. P. Wan, H. T. Lee, C. F. Liu, *Energy Fuels* **2011**, *25*, 890–896.
[18] a) M. Salciccioli, D. G. Vlachos, *ACS Catal.* **2011**, *1*, 1246–1256; b) J. E. Sutton, P. Panagiotopouou, X. E. Veryldos, D. G. Vlachos, *J. Phys. Chem. C* **2013**, *117*, 4691–4706.
[19] J. Zaffran, C. Michel, F. Auneau, F. Delbecq, P. Sautet, *ACS Catal.* **2014**, *4*, 464–468.
[20] S. Wang, V. Vorotnikov, J. E. Sutton, D. G. Vlachos, *ACS Catal.* **2014**, *4*, 604–612.

[21] a) T. R. Munter, T. Bligaard, C. H. Christensen, J. K. Norskov, *Phys. Chem. Chem. Phys.* **2008**, *10*, 5202 – 5206; b) J. Cheng, P. Hu, P. Ellis, S. French, G. Kelly, C. M. Lok, *J. Phys. Chem. C* **2008**, *112*, 1308 – 1311.
[22] M. Salciccioli, M. Stamatakis, S. Caratzoulas, D. G. Vlachos, *Chem. Eng. Sci.* **2011**, *66*, 4319 – 4355.
[23] Y. Chen, M. Salciccioli, D. G. Vlachos, *J. Phys. Chem. C* **2011**, *115*, 18707 – 18720.
[24] a) S. Rangarajan, A. Bhan, P. Daoutidis, *Comput. Chem. Eng.* **2012**, *45*, 114 – 123; b) S. Rangarajan, A. Bhan, P. Daoutidis, *Comput. Chem. Eng.* **2012**, *46*, 141 – 152.
[25] M. A. Christiansen, G. Mpourmpakis, D. G. Vlachos, *ACS Catal.* **2013**, *3*, 1965 – 1975.
[26] W. Gao, W. T. Zheng, Q. Jiang, *J. Chem. Phys.* **2008**, *129*, 164705.
[27] a) C. Zhao, Y. Kou, A. A. Lemonidou, X. B. Li, J. A. Lercher, *Angew. Chem. Int. Ed.* **2009**, *48*, 3987 – 3990; *Angew. Chem.* **2009**, *121*, 4047 – 4050; b) Y. Yoon, R. Rousseau, R. S. Weber, D. H. Mei, J. A. Lercher, *J. Am. Chem. Soc.* **2014**, *136*, 10287 – 10298.
[28] a) G. Kresse, J. Furthmuller, *Phys. Rev. B* **1996**, *54*, 11169 – 11186; b) G. Kresse, J. Furthmuller, *Comput. Mater. Sci.* **1996**, *6*, 15 – 50.
[29] a) J. P. Perdew, K. Burke, M. Ernzerhof, *Phys. Rev. Lett.* **1996**, *77*, 3865 – 3868; b) S. Grimme, J. Antony, S. Ehrlich, H. Krieg, *J. Chem. Phys.* **2010**, *132*, 154104.
[30] a) P. E. Blöchl, *Phys. Rev. B* **1994**, *50*, 17953 – 17979; b) G. Kresse, D. Joubert, *Phys. Rev. B* **1999**, *59*, 1758 – 1775.
[31] C. Kittel, *Introduction to Solid State Physics*, Wiley, New York, **1996**.
[32] H. J. Monkhorst, J. D. Pack, *Phys. Rev. B* **1976**, *13*, 5188 – 5192.
[33] a) G. Mills, H. Jonsson, G. K. Schenter, *Surf. Sci.* **1995**, *324*, 305 – 337; b) G. Henkelman, B. P. Uberuaga, H. Jonsson, *J. Chem. Phys.* **2000**, *113*, 9901 – 9904.

Received: September 2, 2014
Revised: November 2, 2014
Published online on December 2, 2014